Planetary and Space Science 59 (2011) 517–525

Contents lists available at ScienceDirect

Planetary and Space Science

journal homepage: www.elsevier.com/locate/pss

Dipolarization fronts in the magnetotail plasma sheet

A. Runov [a,*], V. Angelopoulos [a], M. Sitnov [b], V.A. Sergeev [c], R. Nakamura [d], Y. Nishimura [e,f], H.U. Frey [g], J.P. McFadden [g], D. Larson [g], J. Bonnell [g], K.-H. Glassmeier [h], U. Auster [h], M. Connors [a,j], C.T. Russell [a], H.J. Singer [i]

[a] Institute of Geophysics and Planetary Physics, University of California, Los Angeles, USA
[b] Applied Physics Laboratory, Johns Hopkins University, Laurel, MD, USA
[c] St. Petersburg State University, St. Petersburg, Russia
[d] Space Research Institute Austrian Academy of Sciences, Graz, Austria
[e] Department of Atmospheric and Oceanic Sciences, University of California, Los Angeles, CA, USA
[f] Solar-Terrestrial Environment Laboratory, Nagoya University, Nagoya, Japan
[g] Space Science Laboratory, University of California, Berkeley, CA, USA
[h] Institute of Geophysics and Extraterrestrial Physics, Technical University Braunschweig, Germany
[i] NOAA Space Weather Prediction Center, Boulder, CO, USA
[j] Athabasca University, Edmonton, AB, Canada

ARTICLE INFO

Article history:
Received 24 September 2009
Received in revised form
13 April 2010
Accepted 9 June 2010
Available online 16 June 2010

Keywords:
Planetary magnetosphere
Plasma sheet
Reconnection

ABSTRACT

We present a THEMIS study of a dipolarization front associated with a bursty bulk flow (BBF) that was observed in the central plasma sheet sequentially at $X=-20.1$, -16.7, and $-11.0R_E$. Simultaneously, the THEMIS ground network observed the formation of a north–south auroral form and intensification of westward auroral zone currents. Timing of the signatures in space suggests earthward propagation of the front at a velocity of 300 km/s. Spatial profiles of current and electron density on the front reveal a spatial scale of 500 km, comparable to an ion inertial length and an ion thermal gyroradius. This kinetic-scale structure traveled a macroscale distance of $10R_E$ in about 4 min without loss of coherence. The dipolarization front, therefore, is an example of space plasma cross-scale coupling. THEMIS observations at different geocentric distances are similar to recent particle-in-cell simulations demonstrating the appearance of dipolarization fronts on the leading edge of plasma fast flows in the vicinity of a reconnection site. Dipolarization fronts, therefore, may be interpreted as remote signatures of transient reconnection.

1. Introduction

Dynamic events in planetary magnetospheres, such as substorms, bursty bulk flows (BBFs), and high-energy particle injections, involve coupling between macro- (global), meso- (typical time scale 1–10 min), and micro-scale (time scale less than 10 s, spatial scale less than or equal to ion gyroradius) processes. Macro-scale interaction between solar wind carrying the interplanetary magnetic field (IMF) and a planetary magnetosphere defines the boundary conditions for meso- and micro-scale processes. Bursty bulk flows (Angelopoulos et al., 1992), a meso-scale phenomenon, may result from a plasma sheet instability (tearing/reconnection, interchange) developed in response to changes in global-scale boundary conditions converting magnetic energy to plasma kinetic energy. Earthward BBFs observed in the plasma sheet within a wide range of geocentric distances from 5 to $30R_E$ are characterized by an increase in the magnetic field Z-component (normal to the undisturbed cross-tail current sheet) and a decrease in plasma density and plasma pressure (Ohtani et al., 2004). Thus, the BBFs display a reduction in plasma tube entropy (pV^{γ}), as described by the bubble model (see Wolf et al., 2009, for review). It is worth noting that entropy-depleted flux tubes (bubbles) are a natural consequence of magnetic reconnection in the magnetotail current sheet (e.g., Wolf et al., 2009). The earthward reconnection outflow carrying an enhanced northward magnetic field ($B_z>0$ in the GSM coordinate system) may reach velocities comparable with the asymptotic Alfvén speed, calculated using the lobe magnetic field (800–1000 km/s) in the reconnection inflow region.

BBFs carrying an enhanced magnetic flux interact with the ambient plasma sheet, which leads to formation of thin boundary layers and a system of field-aligned currents (FACs) that link the BBFs to the ionosphere (e.g., Sergeev et al., 1996; Birn et al., 2004; Nakamura et al., 2004). FAC closure through the ionosphere by the electrojet current results in perturbations in the geomagnetic field observed by ground-based magnetometers (e.g., McPherron et al., 1973). Auroral signatures related to BBFs include polar boundary intensifications (PBI, Zesta et al., 2000) and streamers, often with

* Corresponding author. Tel.: +1 310 2066648.
E-mail address: arunov@igpp.ucla.edu (A. Runov).

0032-0633/$ - see front matter © 2010 Elsevier Ltd. All rights reserved.
doi:10.1016/j.pss.2010.06.006

north–south orientation (Sergeev et al., 2000a, b; Nakamura et al., 2001).

The thin boundary layer separating BBF plasma from the ambient plasma sheet, often observed as a step-like increase in the B_z component, is referred to as a dipolarization front (e.g., Nakamura et al., 2002; Sitnov et al., 2009; Runov et al., 2009). Dipolarization front is comparable to an ion thermal gyroradius (Runov et al., 2009; Sergeev et al., 2009). A dipolarization front is a kinetic-scale plasma structure, a vertical localized current sheet (Sergeev et al., 2009).

In this paper we discuss detailed observations of a dipolarization front associated with a bursty bulk flow detected successively by four THEMIS probes close to the midnight meridian in the plasma sheet. Multi-spacecraft measurements allow us to follow the front's motion from mid-tail to the near-Earth plasma sheet and observe the evolution of its meso- and micro-scale properties. Simultaneous ground-based all-sky camera and magnetometer observations make it possible to identify the front's optical and magnetic signatures in the auroral zone. This combination, along with solar wind/IMF monitoring provided by Cluster, gives a comprehensive picture illustrating multi-scale magnetotail dynamics.

2. Data analysis

2.1. Overview of global (macro) scale observations

We start with a brief overview of space- and ground-based observation between 0700 and 0900 UT on February 27, 2009. The Cluster spacecraft, located in the solar wind upstream of the bow shock, provided monitoring of solar wind and IMF conditions. According to Ion Spectrometer (CIS, Rème et al., 2001) data, the solar wind velocity absolute value at the Cluster spacecraft varied between 450 and 490 km/s. No significant variations in solar wind density were observed. The Cluster Fluxgate Magnetometer (FGM, Balogh et al., 2001) shows that IMF B_z was predominantly northward between 0130 and 0400 UT and between 0440 and 0700 UT. The IMF at Cluster-3 (C3), located at [17.8, 2.2, −11.0] R_E (GSM coordinate system is used throughout this paper), from 0700 to 0900 UT is shown in Fig. 1, panels a–c.

The THEMIS pseudo-AL index, calculated from the THEMIS magnetometer array in Northern America (Russell et al., 2008; Mann et al., 2008), began to increase gradually, while the δB_x (daily median value subtracted) at the CANMOS Yellowknife station (YKC, 69.11°N, 297.9°E, geomagnetic) showed a sharp

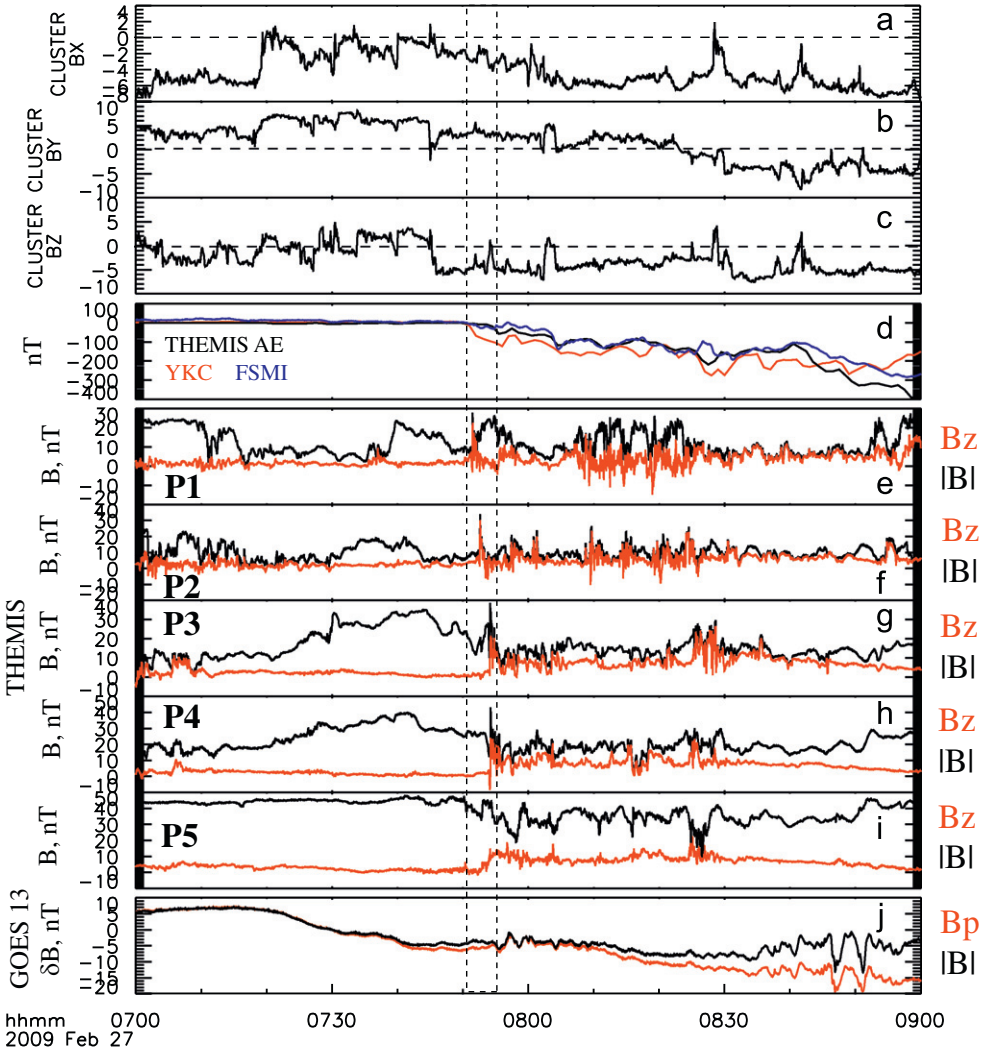

Fig. 1. Overview of space and ground-based magnetic field observations between 0700 and 0900 UT on February 27, 2009: GSM components of the IMF from Cluster 3 (a–c), THEMIS pseudo-AL, δB_x at FSMI (blue) and YKC (red) (d), absolute value and Z-component of the magnetic field from THEMIS spacecraft (e–i), absolute value and p-component at the geosynchronous GOES-13 satellite (j). (For interpretation of the references to color in this figure legend, the reader is referred to the web version of this article.)

decrease at about 0750 UT (panel d). This sharp δB_x was not detected by the magnetometer at Fort Smith (FSMI, 67.21N, 306.64E), which indicates that the corresponding current system was very localized.

The Flux-Gate Magnetometer (FGM, Auster et al., 2008) at THEMIS probes P1–P4 (panels e–h), situated in the plasma sheet ($|B| < 10$ nT at P1, P2 and < 30 nT at P3, P4), detected high-amplitude spikes in both the Z-component and the absolute value of the magnetic field (a dashed-line box in Fig. 1). The spikes were detected by P1 at 0751:26 UT, then by P2 at 0752:34 UT, and, finally by P3 and P4 at 0754:07 and 0754:11 UT, respectively (see Fig. 2 for probe locations). Assuming that the variations are due to propagation of a spatial structure (a dipolarization front), the timing suggests an earthward propagation velocity of 300 km/s

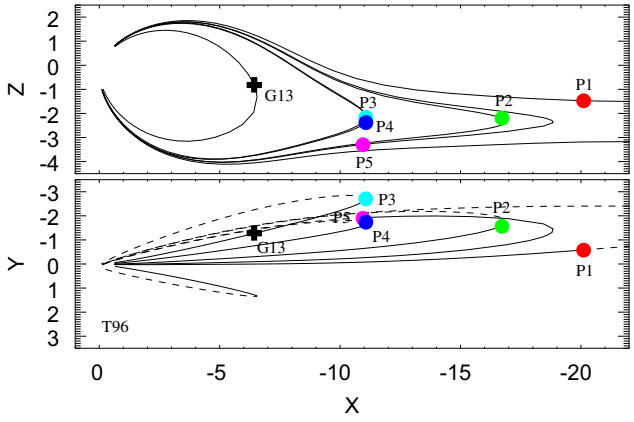

Fig. 2. THEMIS (P1–P5) and GOES 13 (G13) spacecraft locations at 0750 UT on February 27, 2009, are shown along with T96-model field lines.

(Runov et al., 2009). THEMIS P5 (panel i), which was away from the central plasma sheet, detected a more gradual, smaller-amplitude increase in B_z. The GOES-13 spacecraft, situated on geosynchronous orbit in conjunction with THEMIS probes, detected small-amplitude Pi2-like variations in the magnetic field (panel j).

Fig. 3 (left column) shows two successive mosaics of auroral images obtained by a group of THEMIS All-Sky Imagers (ASI, Mende et al., 2008) located near magnetic midnight. Footprints of the THEMIS probes, estimated by mapping the probe positions onto the ionosphere along the T96 (Tsyganenko, 1995) model magnetic field lines, were near midnight and in the field of view of the ASI stations. (The entire mosaic as well as individual images from all stations is available at http://themis.ssl.berkeley.edu/gbo/.) Pronounced intensification was observed at 0747 UT at Fort Smith and Gillam. The aurora progressed poleward between 0749:30 and 0752:30 UT. The formation of a north–south (NS) structure, a part of an auroral vortex visible in the Fort Smith field of view, began at 0752:30. This structure appeared at about 70° (see image taken at 0752:30 UT), somewhat south of the polar boundary of the auroral oval.

The right column in Fig. 3 shows Earth magnetic field variations detected by YKC between 0745 and 0800 UT. The variations in X (northward) and Z (vertical down) components, indicating a growth of westward electrojet, started at 0749:48 UT (prior to the dipolarization front detection) southward of YKC. A pronounced negative variation in B_z was observed between 0753:50 and 0756:50 UT, i.e., about 2 min after the dipolarization front was observed by P1. This may indicate a poleward expansion of the electrojet.

2.2. THEMIS meso-scale observations

In this subsection we describe and analyze magnetic field and particle observations made by four THEMIS probes (P1–P4) in the

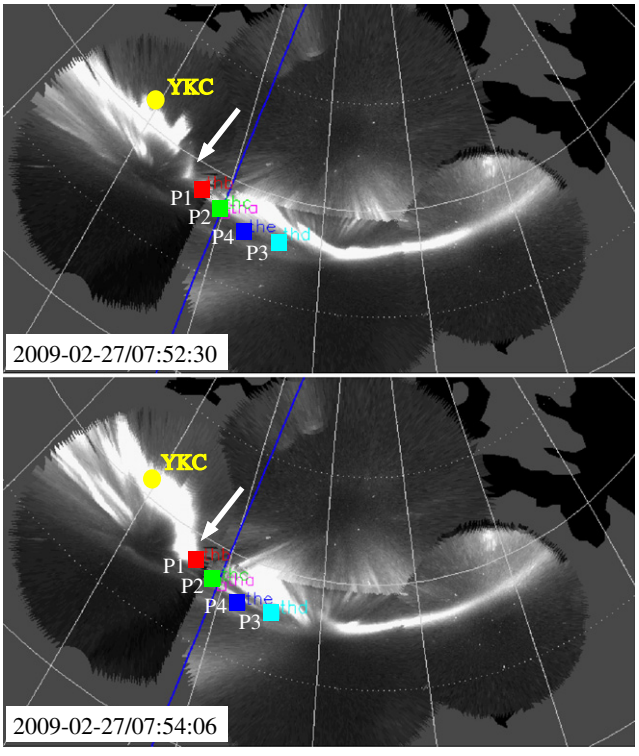

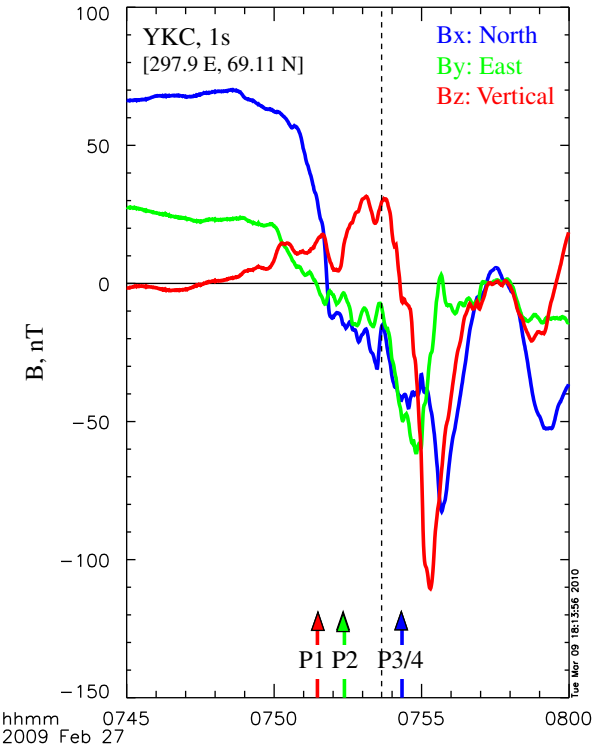

Fig. 3. Left column: snapshots of THEMIS all-sky camera auroral images at 0752:30 and 0754:06 UT. Coordinates are geographic. THEMIS P1, P2, P3, and P4 footprints are calculated using the T96 model. The blue line indicates magnetic midnight. The white arrow points to the NS auroral structure (see text for details). Right column: variations in X, Y, and Z magnetic field components observed at the CANMOS Yellowknife station. Vertical lines indicate times of the dipolarization front observations by THEMIS P1, P2, P3, and P4. (For interpretation of the references to color in this figure legend, the reader is referred to the web version of this article.)

plasma sheet, focusing on variations with several-minute time scales (meso-scale). Particle data are provided by the THEMIS Electrostatic Analyzer (ESA, McFadden et al., 2008), which measures ion and electron fluxes in the energy range 0–28 keV, and by the Solid State Telescope (SST, Angelopoulos, 2008), which covers the energy range 30 to ~1000 keV. Since the burst-mode data are available during the interval of interest, both instruments provide data with a ~3 s sampling rate and full angular resolution (ESA: $32\times11.25^\circ$, 8×22.5, SST: $16\times22.5^\circ$, $4\times30^\circ$).

Fig. 4 shows the magnetic field and the plasma parameters observed by P1 at $[-20.1,\ -0.6,\ -1.5]R_E$ and by P2 at $[-16.7,\ -1.6,\ -2.2]R_E$ for 5 min between 0750 and 0755 UT. At around the dipolarization front arrival time (indicated by dashed vertical lines), both probes observed similar plasma parameter behavior, including a drop in plasma density from ~1 to ~0.1 cm^{-3}, an increase in electron temperature from 0.3 to 1.5 keV, and an increase in perpendicular proton temperature ($T_\perp$) from 2 to 5–6 keV. The increase in $T_\perp$, which lasted about a minute, was followed by an increase in the parallel proton temperature. The plasma bulk velocity at both probes was modest at front arrival and increased gradually behind the front. Although the ion temperature increased behind the front, the plasma pressure decreased due to the density drop. The plasma-$\beta=2\mu_0P_iB^{-2}$ at P1 and P2 was larger than 10 prior to arrival of the dipolarization front. The aforementioned decrease in plasma pressure along with an increase in total magnetic field value causes a decrease in β at the front to ~1. Similar behavior of β was previously shown for flux ropes (e.g., Slavin et al., 2005). The flux-tube entropy function $PV^{5/3}$, where V is the flux tube volume, calculated using the Wolf et al. (2006) approach, decreased from ≈0.2 to ≈0.05 $(nPa\cdot R_E/nT)^{5/3}$. It should be noted, however, that the Wolf et al. (2006) formalism, which was developed assuming the force balance, may be inaccurate for high-speed flow intervals. Since the bulk flow velocity increased gradually, we applied the technique to qualitatively estimate the flux-tube entropy ahead of and behind the front. Both probes also detected a notable increase in differential energy fluxes (DEF, eV $[s\,cm^2\,sr\,eV]^{-1}$) of 50–200 keV ions and a jump in differential energy fluxes of 30–150 keV electrons.

The dipolarization front, therefore, is a boundary separating hot, tenuous, lower-entropy BBF plasma with significantly anisotropic ion temperature from the relatively dense, cool, higher-entropy, isotropic ambient plasma sheet.

Observations made by P3 at $[-11.1,\ -2.8,\ -2.2]$ and P4 at $[-11.1,\ -1.8,\ -2.4]R_E$ between 0752 and 0757 UT are shown in Fig. 5. Generally, these two probes, separated mainly in the Y-direction, observed signatures similar to those detected by P1 and P2 2–3 min earlier: a drop in plasma density, an increase in electron temperature, a gradual increase in bulk velocity, a decrease in flux-tube entropy function, a gradual increase in 100–300 keV ion DEFs, and a sharp increase in 30–200 keV electron DEFs. Thus, the P3/P4 pair situated in the near-Earth plasma sheet observed the same boundary that had been detected earlier in the mid-tail plasma sheet. At the same time, there are notable differences in P3 and P4 observations. The bulk flow velocity at P3 was tailward and dawnward ahead of the front, but turned earthward whereas at P4 it was mainly earthward with a significant duskward component just ahead of the front. The ion temperature at P3 gradually increased from 3 to 4 keV, whereas at P4 its behavior was similar to that at P1 and P2 (a rapid jump with significant anisotropy ($T_\perp > T_\parallel$) lasted about a minute). Since P3 and P4 probes were located at the same X and Z, these differences should be attributed to their Y-separation.

2.3. THEMIS micro-scale observations

This subsection is focused on micro-scale properties of the dipolarization front, a boundary separating BBF plasma from

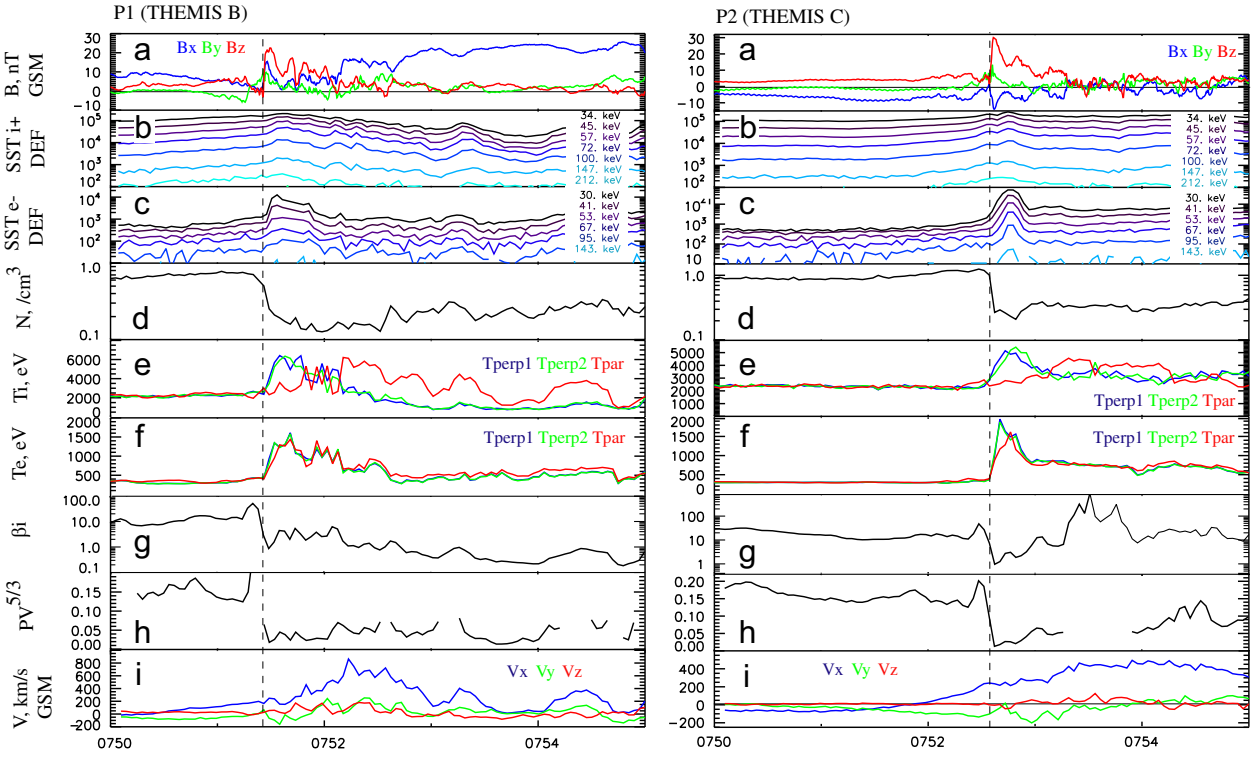

Fig. 4. Observations by THEMIS P1 (left column) and P2 (right column) between 0750 and 0755 UT on February 27, 2009. For each probe plot from top to bottom: GSM components of the magnetic field (a), ion (b), and electron (c) differential energy fluxes at energies >30 keV, plasma density (d), ion (e), and electron (f) temperatures, plasma β parameter (g), flux-tube entropy function (h), and bulk flow velocity (i).

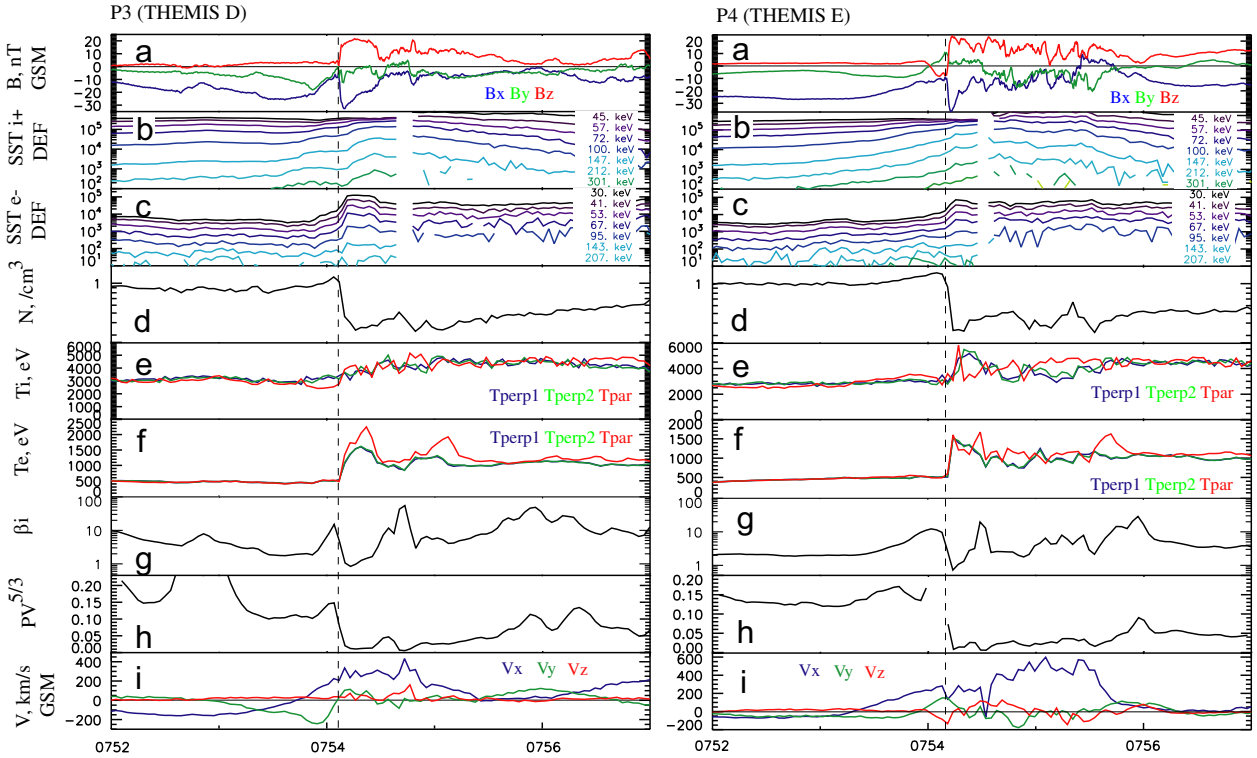

Fig. 5. Observations by THEMIS P3 (left column) and P4 (right column) between 0752 and 0757 UT on February 27, 2009. The same format as in Fig. 4.

ambient media. Burst-mode data with the highest temporal resolutions (128 Hz for FGM and the spin-resolution (~ 3 s) for ESA and SST) allow us to reconstruct a detailed spatial profile of the front. Assuming a constant, earthward-directed propagation velocity $V_t \approx 300$ km/s, the integral $\Delta X = \int_{t_0}^{t} V_t\, d\tau$ gives the distance traveled by the spacecraft in the tailward direction across the front. The Y-component of the current density $j_y = \mu_0^{-1}[\partial_z B_x - \partial_x B_z] = j_{y0} + j_{y1}$ is the sum of the equatorial current density (j_{y0}) and the current density associated with the dipolarization front (j_{y1}). An estimate of j_{y0} may be obtained by comparing B_x at P1 and P2 at the front: ≈ 5 and ≈ -5 nT, respectively. The Z-distance between the two probes was $\Delta Z \approx 4.5 \times 10^3$ km. Assuming planar geometry of the cross-tail current sheet, this gives an estimate of $j_{y0} \approx 2$ nA/m^2. The term (j_{y1}) may be estimated from temporal variations in B_z and V_t: $j_{y1} \approx \mu_0^{-1} \Delta B_z / V_t \Delta t$, where ΔB_z is the variation in B_z during the time interval Δt. Fig. 6 shows B_z, j_{y1} and the electron number density (n_e) estimated from the spacecraft potential (e.g., Mozer, 1973), measured by the THEMIS Electric Field Instrument (EFI, Bonnell et al., 2008), plotted against the tailward distance ΔX traveled by P1 and P2. The maximum values of j_{y0} reached ~ 100 nA/m^2 at P1 and ~ 70 nA/m^2 at P2 are two orders of magnitude larger than j_{y0}. The j_{y1} profiles at P1 and P2 reveal a similar structure, including a negative peak (more pronounced at P2) and two positive peaks. The 500 km scale of the double-peak structure corresponds to that of the electron density gradient. The negative peak of j_{y1} was observed slightly ahead of the n_e gradient.

Row (d) in Fig. 6 contains a set of electron distribution functions obtained by P1 and P2 ESA (0.1–25 keV energy range; points with count rate below 1 count/s are excluded) ahead of the front, in close proximity to it, and behind it. Although some details of the observed distributions are different at P1 and P2, it is clear that the electron population behind the front is more energetic and has a pancake-like distribution (90° electrons are more energetic than 0° and 180° ones). A corresponding set of high-energy (28–200 keV) electron pitch-angle distributions (PAD) obtained by P1 and P2 SST is displayed in row (e). The PAD at P1 and P2 show the same feature: 90° electrons of energies >30 keV on and behind the front.

Fig. 7 shows the same observations but for P3 and P4. $j_{y0} \propto \Delta Bx/\Delta Z$ estimated from differences between P3/P4 and P4/P5 did not exceed 3 nA/m^2 at the front. Thus, the cross-tail current density was dominated by $j_{y1} \propto \Delta Bz/\Delta X$. The profile observed by P3 reveals the same structure (with a negative and two positive peaks in j_{y1}) as was observed 3 and 2 min earlier by P1 and P2. The j_{y1} profile at P4 looks different. At P4 the front-normal direction obtained via MVA deviated from the bulk velocity direction (Runov et al., 2009). Thus, P4 might cross the front partly tangentially, which may explain the difference in j_{y1} profiles at P3 and P4.

The electron distribution functions obtained ahead of, around, and behind the front show similar properties at P3 and P4, including more isotropic heating, than observed by P1 and P2. The corresponding PAD of high-energy electrons also differ from those at P1/P2. At P3, the PAD of >30 keV electrons obtained at and behind the front exhibit peaks at 0°, 90°, and 180°. At P4, the PAD are rather cigar-shaped with peaks at 0° and 180°.

3. Summary and discussion

We have shown a set of space- and ground-based observations illustrating macro-, meso-, and micro-scale plasma sheet characteristics during a bursty-bulk flow event. IMF variations between 0700 and 0730 UT (see Fig. 1) may change global-scale boundary conditions. Some plasma sheet instability, presumably reconnection, which may act in response to the change in global boundary conditions, led to formation of a meso-scale object, a flux tube populated by hot, tenuous, earthward-moving plasma with lower PV^{γ}, carrying an enhanced magnetic flux through the equatorial

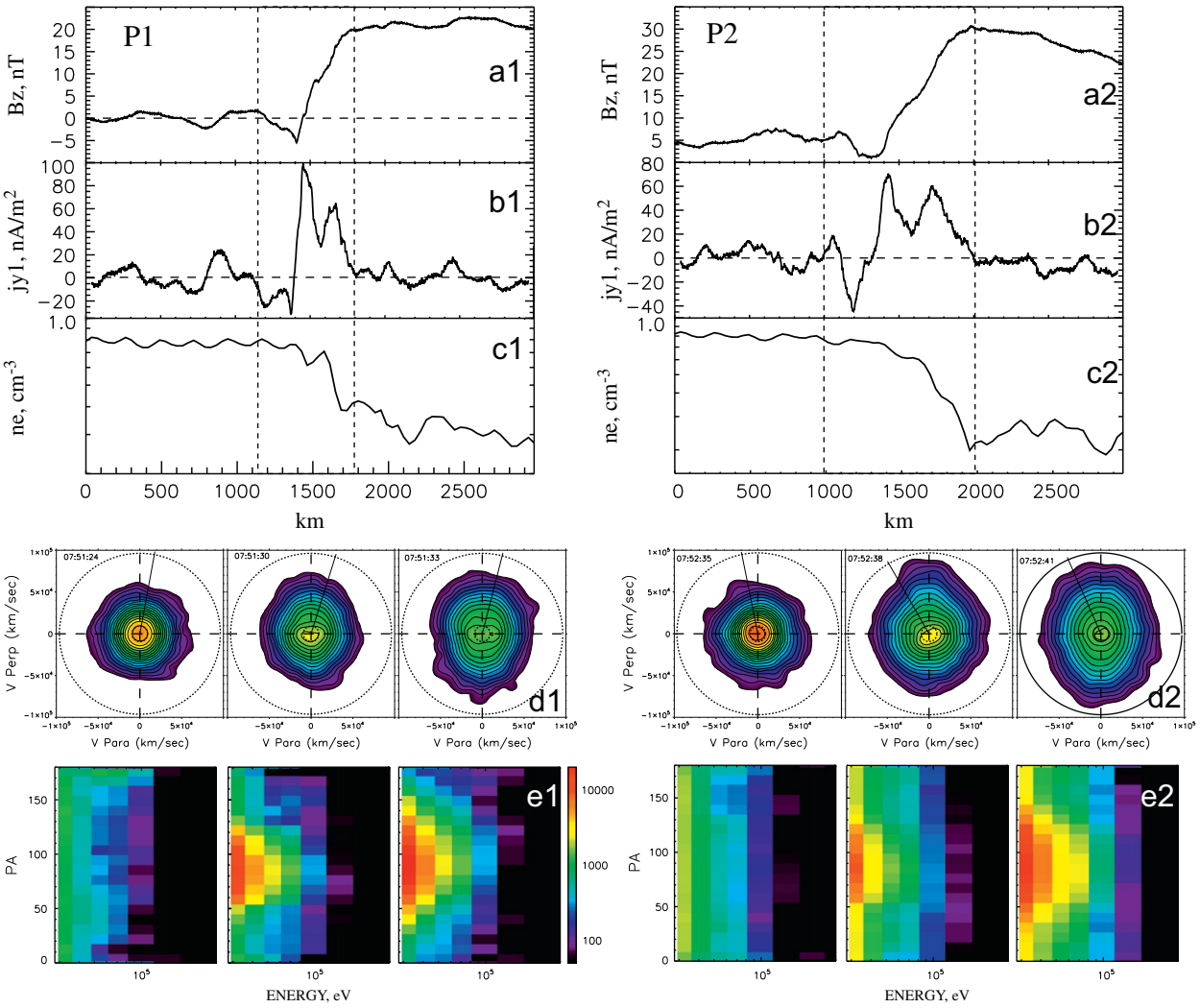

Fig. 6. Reconstructed spatial profiles of B_z, $j_{y1}=\mu_0^{-1}\Delta B_z/\Delta x$, and electron density n_e at P1 and P2 (rows a, b, and c) on the dipolarization front. (d) 0.1–25 keV (ESA) electron distribution functions in the ($V_\parallel$, $V_\perp$) obtained ahead of the front, on it, and behind it. Phase space density (s^3/cm^6) is color-coded. (e) Corresponding 30–200 keV electron (SST) pitch-angle distributions, differential energy flux ($eV/s/cm^2/sr/eV$) is color-coded. (For interpretation of the references to color in this figure legend, the reader is referred to the web version of this article.)

plane, i.e., a plasma bubble. The new plasma population was detected successively by THEMIS probes situated in the plasma sheet, starting with the most distant one (P1). The quantitative and qualitative similarity in field and plasma parameters observed successively at $X=-20$, -16, and $-11R_E$ suggests that the same plasma bubble was observed successively in the course of its earthward propagation. The propagation velocity, estimated to be 300 km/s, is consistent with recent observations by the Cluster and Double Star spacecraft (Walsh et al., 2009), although smaller than the propagation velocity of the transient dipolarization reported by Slavin et al. (2002). The bubble was observed by each probe for ($\sim$1 min). An estimation of its scale in the X-direction is therefore 2.5–3R_E.

A distinct auroral structure, oriented mainly in the north-south direction, was observed by the THEMIS ASI station in the near-midnight sector about a minute after the first observation of the new plasma population in the plasma sheet by P1. This auroral structure was likely an ionospheric manifestation of the BBF. Enhancement of the westward electrojet observed in the same MLT sector as THEMIS probe footpoints $\sim$150 s later than detection of the dipolarization front by P1 (Fig. 3) may be interpreted as a signature of a localized BBF-related FAC system.

A micro-scale boundary, the dipolarization front was formed by interaction between the BBF and the ambient plasma sheet. It was detected successively by spacecraft located in the plasma sheet between $X=-20$ and $-11R_E$. The inward propagation of the transient dipolarization agrees with previous observations by radially separated spacecraft (e.g., Ohtani, 1998; Slavin et al., 2002). Since it was not observed by GOES-13, situated in conjunction with THEMIS (Figs. 1 and 2), the front likely stopped somewhere between $-11R_E$ and geosynchronous orbit. Pi2-like variations in the magnetic field observed by the geostationary spacecraft indicate that a compression wave was launched by braking of the BBF.

Spatial reconstruction of the dipolarization front profile (Figs. 6 and 7) shows that the B_z variation and the positive cross-tail current density nearly coincide with a rapid decrease in electron density, although the major n_e gradient started slightly behind the first peak in j_y. Similar observations were recently reported by Sergeev et al. (2009). The scales of both the current density and electron density gradient were similar (estimated to be $\sim$500 km), on the order of magnitude of the 5-keV proton gyroradius in the magnetic field of 20 nT. This 500-km scale, which is also comparable to the ion inertial scale $d_i=c/\omega_{pi}$ for $n_i=0.2\,cm^{-3}$, suggests electron and ion decoupling. The electric current due to dawnward net drift of electrons on the sharp pressure gradient (diamagnetic current) may support the sharp

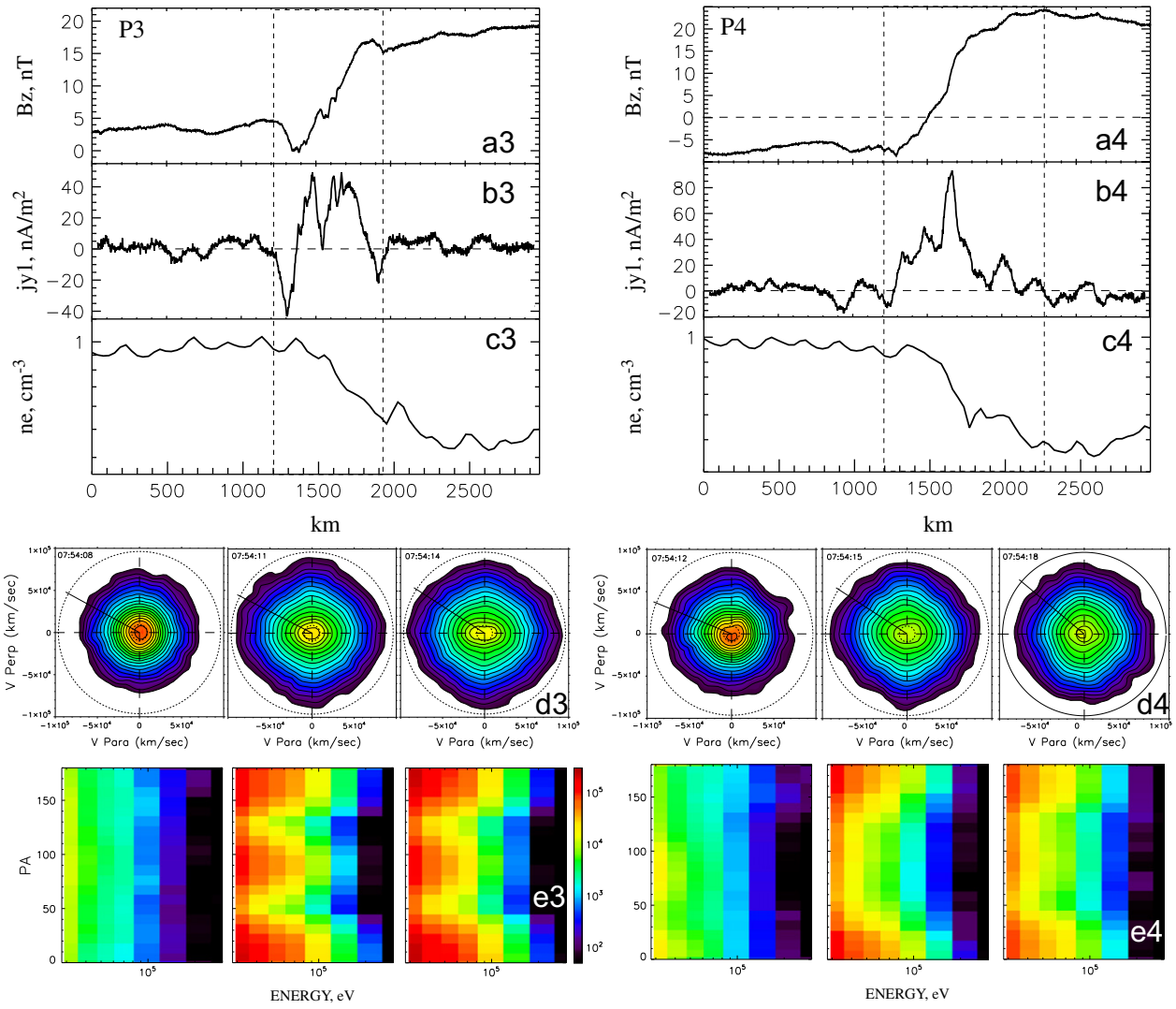

Fig. 7. The same as in Fig. 6 at P3 and P4.

positive variation in B_z. Quantitatively, an 0.1 nPa jump in pressure over a distance of 500 km in the 20 nT-field results in a diamagnetic current density of 10 nA/m^2, assuming that ions are stationary. A B_z variation of 20 nT over 500 km gives $j_y \sim 30$ nA/m^2. That ∇B_z and ∇n_e do not fully coincide suggests that local particle acceleration may significantly contribute to the current density. The negative j_y observed ahead of the front may be due to electrons drifting duskward in the magnetic field gradient. The local observations do not provide information on the closure of these currents. The westward electrojet signatures detected by the ground-based magnetometer (Fig. 3) suggest closure through ionosphere via FACs.

Enhancements in the 50–200 keV ion and 30–150 keV electron energy fluxes were observed on the dipolarization front. A gradual increase in ion energy flux was detected ahead of the front and a more rapid increase observed after it. The energy flux of high-energy electrons, in contrast, increased exactly at the front. Interestingly, at $-20 < X < -16R_E$, the pitch-angle distribution of the electron energy flux shows a maximum at 90°, whereas at $X = -11R_E$ the PAD reveals maxima at 0° and 180°. The dipolarization front, therefore, is an earthward-propagating boundary of energetic particle intrusion. In this sense, it may be referred to as "injection boundary" (e.g., Moore et al., 1981; Sergeev et al., 2009; Zhou et al., 2009).

Recently, the formation of dipolarization fronts was demonstrated in PIC simulations of impulsive reconnection with open boundary conditions (Sitnov et al., 2009). Fig. 8 shows the simulation results: localized intensifications of the cross-tail current density (dipolarization fronts) are clearly visible in negative (dashed box) and positive halves of the simulation domain. The simulation results reveal many features that are similar to those in our observations: the front thickness is about d_i; the electric field component normal to the front, which suggests ion and electron decoupling at the front; plasma density increase followed by abrupt decrease, and a more gradual increase in plasma bulk velocity (see Fig. 8, right column). In the simulations, the fronts appeared at a short distance ($< 20d_i$) from the initial X-line. The similarity with observations indicates that fronts generated in the course of transient reconnection may survive a long time and travel macroscopic distances. The simulations also showed that energy dissipation ($\mathbf{j} \cdot \mathbf{E}$) is stronger on the dipolarization fronts than at the initial reconnection region. Recent PIC simulations of magnetopause reconnection also showed that the dissipation region where electrons are energized has an ion scale size and are not co-located with the reconnection region (Pritchett and Mozer, 2009). THEMIS observations indeed show acceleration of ions ahead of the front (Zhou et al., 2010). More efforts, both in modeling and

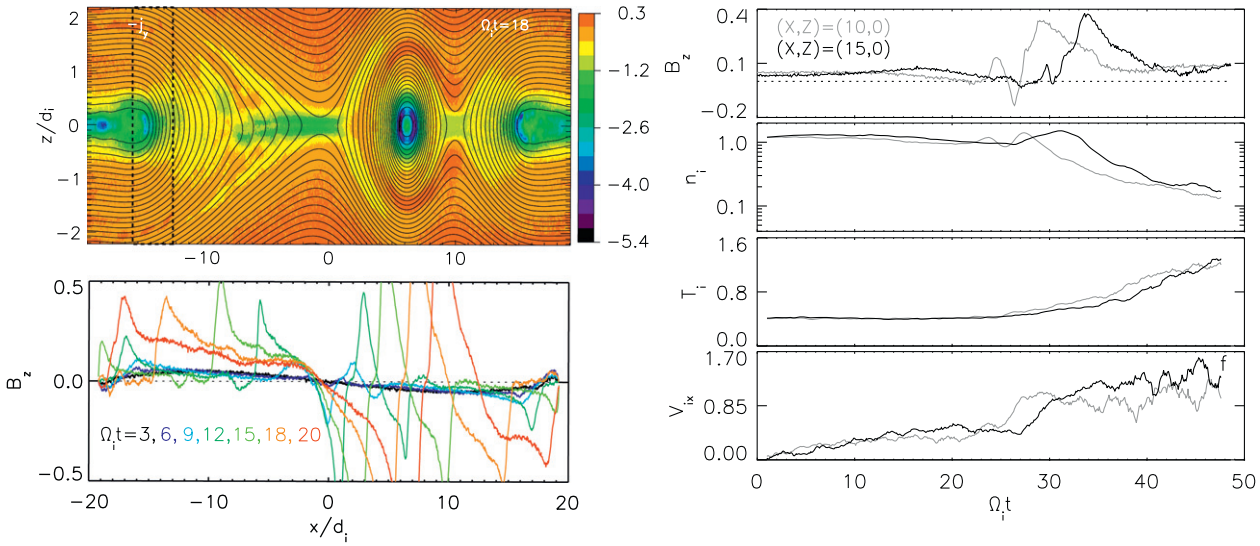

Fig. 8. Left column: a snapshot of magnetic field (lines) and current density (color-coded) resulting from PIC simulations with open boundary conditions (Sitnov et al., 2009). A set of B_z profiles at different times. The dipolarization front is indicated by dashed box. Right column: time-series of field and particle parameters as measured by two virtual probes in the simulation box. Compare with Figs. 4 and 5. (For interpretation of the references to color in this figure legend, the reader is referred to the web version of this article.)

data analysis, are needed to separate local energization from transport of pre-energized particles.

4. Concluding remarks

Showing the clearest example of a dipolarization front, our case is not unique. THEMIS observations during the 2008–2009 magnetotail seasons reveal many similar events.

Although THEMIS multi-probe observations allow us to reconstruct a one-dimensional profile of the dipolarization front, assuming its earthward propagation at a constant velocity, multi-point measurements with small separations along all three directions are needed to resolve the three-dimensional structure of dipolarization fronts. This is also a topic to be addressed in future multi-spacecraft magnetospheric missions, such as MMS, Scope, and Cross-Scale.

The kinetic model of transient magnetic reconnection may explain many observed signatures. Understanding of the structure and closure of the current system supporting the dipolarization front requires three-dimensional modeling, however. The stability of this system and the mechanisms of particle acceleration and heating on the front should be addressed in further theoretical analyses.

Acknowledgements

We acknowledge NASA contracts NAS5-02099 and NNX08AD85G, the German Ministry for Economy and Technology and the German Center for Aviation and Space (DLR), contract 50 OC 0302. We thank P.L. Pritchett and L. Lyons for discussions; D. Danskin for providing NRCan CANMOS data; E. Lucek and I. Dandouras for providing Cluster FGM and CIS data; B. Kerr, P. Cruce, M. Feuerstein, E. Penou and J. Hohl for help with software and editing.

References

Angelopoulos, V., 2008. The THEMIS mission. Space Sci. Rev. 141, 5–34.

Angelopoulos, V., Baumjohann, W., Kennel, C.F., Coroniti, F.V., Kivelson, M.G., Pellat, R., Walker, R.J., Lühr, H., Paschmann, G., 1992. Bursty bulk flows in the inner central plasma sheet. J. Geophys. Res. 97, 4027–4039.

Auster, H.U., Glassmeier, K.H., Magnes, W., Aydogar, O., Baumjohann, W., Constantinescu, D., Fischer, D., Fornacon, K.H., Georgescu, E., Harvey, P., Hillenmaier, O., Kroth, R., Ludlam, M., Narita, Y., Nakamura, R., Okrafka, K., Plaschke, F., Richter, I., Schwarzl, H., Stoll, B., Valavanoglou, A., Wiedemann, M., 2008. The THEMIS fluxgate magnetometer. Space Sci. Rev. 141, 235–264.

Balogh, A., Carr, C.M., Acuña, M.H., Dunlop, M.W., Beek, T.J., Brown, P., Fornacon, K.-H., Georgescu, E., Glassmeier, K.-H., Harris, J., Musmann, G., Oddy, T., Schwingenschuh, K., 2001. The Cluster magnetic field investigation: overview of in-flight performance and initial results. Ann. Geophys. 19, 1207–1217.

Birn, J., Raeder, J., Wang, Y.L., Wolf, R.A., Hesse, M., 2004. On the propagation of bubbles in the geomagnetic tail. Ann. Geophys. 22, 1773–1786.

Bonnell, J.W., Mozer, F.S., Delory, G.T., Hull, A.J., Ergun, R.E., Cully, C.M., Angelopoulos, V., Harvey, P.R., 2008. The electric field instrument (EFI) for THEMIS. Space Sci. Rev. 141, 303–341.

Mann, I.R., Milling, D.K., Rae, I.J., Ozeke, L.G., Kale, A., Kale, Z.C., Murphy, K.R., Parent, A., Usanova, M., Pahud, D., Lee, E.-A., Angelopoulos, V., Russell, C.T., Singer, H., 2008. The upgraded CARISMA magnetometer array in the THEMIS era. Space Sci. Rev. 141, 413–451.

McFadden, J.P., Carlson, C.W., Larson, D., Angelopolos, V., Ludlam, M., Abiad, R., Elliot, B., 2008. The THEMIS ESA plasma instrument and in-flight calibration. Space Sci. Rev. 141, 277–302.

McPherron, R.L., Russell, C.T., Aubry, M.A., 1973. Satellite studies of magneto-spheric substorms on August 15, 1968, 9, phenomenological model for substorms. J. Geophys. Res. 78, 3131–3149.

Mende, S.B., Harris, S.E., Frey, H.U., Angelopoulos, V., Russell, C.T., Donovan, E., Jackel, B., Greffen, M., Peticolas, L.M., 2008. The THEMIS array of ground-based observatories for the study of auroral substorms. Space Sci. Rev. 141, 357–387.

Moore, T., Arnoldy, R., Feynman, J., Hardy, D., 1981. Propagating substorm injection fronts. J. Geophys. Res. 86, 6713–6726.

Mozer, F.S., 1973. Analysis of techniques for measuring DC and AC electric fields in the magnetosphere. Space Sci. Rev. 14, 272–313.

Nakamura, R., Baumjohann, W., Brittnacher, M., Sergeev, V.A., Kubyshkina, M., Mukai, T., Liou, K., 2001. Flow bursts and auroral activations: onset timing and foot point location. J. Geophys. Res. 106, 10777–10789.

Nakamura, R., Baumjohann, W., Klecker, B., Bogdanova, Y., Balogh, A., Re'me, H., Bosqued, J.M., Dandouras, I., Sauvaud, J.-A., Glassmeier, K.-H., Kistler, L., Mouikis, C., Zhang, T.L., Eichelberger, H., Runov, A., 2002. Motion of the dipolarization front during a flow burst event observed by Cluster. Geophys. Res. Lett. 29, 1942. doi:10.1029/2002GL015763.

Nakamura, R., Baumjohann, W., Nagai, T., Fujimoto, M., Mukai, T., Klecker, B., Treumann, R., Balogh, A., Rème, H., Sauvaud, J.-A., Kistler, L., Mouikis, C., Owen, C.J., Fazakerley, A.N., Dewhurst, J.P., Bogdanova, Y., 2004. Flow shear near the boundary of the plasma sheet observed by Cluster and Geotail. J. Geophys. Res. 109, A05204, doi:10.1029/2003JA010174.

Ohtani, S., 1998. Earthward expansion of tail current disruption: dual-satellite study. J. Geophys. Res. 103, 6815–6825.

Ohtani, S.I., Shay, M.A., Mukai, T., 2004. Temporal structure of the fast convective flow in the plasma sheet: comparison between observations and two-fluid simulations. J. Geophys. Res. 109.

Pritchett, P.L., Mozer, F.S., 2009. The magnetic field reconnection site and dissipation region. Phys. Plasmas 16, 080702.

Rème, H., Aoustin, C., Bosqued, J.M., Dandouras, I., Lavraud, B., Sauvaud, J.-A., Barthe, A., Bouyssou, J., Camus, T., Coeur-Joly, O., et al., 2001. First

multispacecraft ion measurements in and near the Earth's magnetosphere with the identical Cluster ion spectrometry (CIS) experiment. Ann. Geophys. 19, 1303–1354.

Runov, A., Angelopoulos, V., Sitnov, M.I., Sergeev, V.A., Bonnell, J., McFadden, J.P., Larson, D., Glassmeier, K.-H., Auster, U., 2009. THEMIS observations of an earthward-propagating dipolarization front. Geophys. Res. Lett. 36, L14106, doi:10.1029/2009GL038980.

Russell, C.T., Chi, P.J., Dearborn, D.J., Ge, Y.S., Kuo-Tiong, B., Means, J.D., Pierce, D.R., Rowe, K.M., Snare, R.C., 2008. THEMIS ground-based magnetometers. Space Sci. Rev. 141, 389–412.

Sergeev, V., Angelopoulos, V., Apatenkov, S., Bonnell, J., Ergun, R., McFadden, J., Larson, D., Nakamura, R., Runov, A., 2009. Structure of injection front in the flow braking region. Geophys. Res. Lett. 36, L21105, doi:10.1029/2009GL040658.

Sergeev, V.A., Angelopulous, V., Gosling, J.T., Cattell, C.A., Russell, C.T., 1996. Detection of localized, plasma-depleted flux tubes or bubbles in the midtail plasma sheet. J. Geophys. Res. 101, 10817–10826.

Sergeev, V.A., Sauvaud, J.-A., Popescu, D., Kovrazhkin, R.A., Liou, K., Newell, P., Brittnacher, M., Parks, G.R.N., Mukai, T., Reeves, G.D., 2000a. Multiple-spacecraft observation of a narrow transient plasma jet in the Earth's plasma sheet. Geophys. Res. Lett. 27, 851–855.

Sergeev, V.A., Sauvaud, J.-A., Popescu, D., Kovrazhkin, R.A., Lutsenko, V.N., Zelenyi, L.M., Syrjasuo, M., Viljanen, A., Pulkkinen, T.I., Kudela, K., Kokubun, S., Mukai, T., 2000b. Plasma sheet ion injections into the auroral bulge: correlative study of spacecraft and ground observations. J. Geophys. Res. 105, 18465–18482.

Sitnov, M.I., Swisdak, M., Divin, A.V., 2009. Dipolarization fronts as a signature of transient reconnection in the magnetotail. J. Geophys. Res. 114, A04202, doi:10.1029/2008JA013980.

Slavin, J.A., Fairfield, D.H., Lepping, R.P., Hesse, M., Ieda, A., Tanskanen, E., Østgaard, N., Mukai, T., Nagai, T., Singer, H.J., Sutcliffe, P.R., 2002. Simultaneous observations of earthward flow bursts and plasmoid ejection during magnetospheric substorms. J. Geophys. Res. 107, 1106, doi:10.1029/2000JA003501.

Slavin, J.A., Tanskanen, E.I., Hesse, M., Owen, C.J., Dunlop, M.W., Imber, S., Lusek, E.A., Balogh, A., Glassmeier, K.-H., 2005. Cluster observations of travelling compression regions in the near-tail. J. Geophys. Res. 30, A06207, doi:10.1029/2004JA010878.

Tsyganenko, N.A., 1995. Modeling the Earth's magnetospheric magnetic field confined within a realistic magnetopause. J. Geophys. Res. 100, 5599–5612.

Walsh, A.P., Fazakerley, A.N., Lahiff, A.D., Volwerk, M., Grocott, A., Dunlop, M.W., Lui, A.T.Y., Kistler, L.M., Lester, M., Mouikis, C., Pu, Z., Shen, C., Shi, J., Taylor, M.G.G.T., Lucek, E., Zhang, T.L., Dandouras, I., 2009. Cluster and double star multipoint observations of a plasma bubble. Ann. Geophys. 27, 725–743.

Wolf, R.A., Kumar, V., Toffoletto, F.R., Erickson, G.M., Savoie, A.M., Chen, C.X., Lemon, C.L., 2006. Estimating local plasma sheet PV5/3 from single spacecraft observations. J. Geophys. Res. 111, A12218, doi:10.1029/2006JA012010.

Wolf, R.A., Wan, Y., Xing, X., Zhang, J.-C., Sazykin, S., 2009. Entropy and plasma sheet transport. J. Geophys. Res. 114, A00D05, doi:10.1029/2009JA014044.

Zesta, E., Lyons, L.R., Donovan, E., 2000. The auroral signature of earthward flow bursts observed in the magnetotail. Geophys. Res. Lett. 27, 3241–3244.

Zhou, M., Ashour-Abdalla, M., Deng, X., Schriver, D., El-Alaoui, M., Pang, Y., 2009. THEMIS observation of multiple dipolarization fronts and associated wave characteristics in the near-Earth magnetotail. Geophys. Res. Lett. 136, L20107, doi:10.1029/2009GL040663.

Zhou, X.-Z., Angelopoulos, V., Sergeev, V.A., Runov, A., 2010. Accelerated ions ahead of Earthward-propagating dipolarization fronts. J. Geophys. Res., in press, doi:10.1029/2010JA015481.